Lactone-layered double hydroxide networks: Towards self-assembled bioscaffolds

Lactone-Layered Double Hydroxide Networks: Towards Self-Assembled Bioscaffolds

Tianhao Zhou[1], Edward D. McCarthy[2]*, Constantinos Soutis[1], Sarah H. Cartmell[1]

1. School of Materials, The University of Manchester, Oxford Road, Manchester, M13 9AX, UK.

2. School of Engineering, The University of Edinburgh, Sanderson Building, Kings Buildings, Edinburgh, EH9 3GL, UK.

Abstract

This paper describes the conversion of a layered anionic initiator (carbonate-intercalated layered double hydroxide, (LDH-carbonate)) into a self-assembled resin-embedded network during the in-situ polymerisation of one or more lactone monomers using the LDH-carbonate as the sole initiator. Uniquely in this paper, no long-chain acid intercalant is present in the LDH-carbonate to act as an additional initiator species, and this is the first known report of a copolymerisation of these lactones using LDH as an initiator. The formation of a network is in marked contrast to the behaviour of most in-situ polymerisations using layered species, where the latter retains its layered structure at the molecular level and is either intercalated or exfoliated to form a nanocomposite. The molecular disintegration of the LDH sheets is unusual. Nine new insoluble materials (scaffolds) are isolated from various L,D-lactide & ε-caprolactone (LC) and L,D-lactide & δ-valerolactone (LV) copolymer hybrids. The latter hybrids are polymerised using the LDH-carbonate as initiator at 150 °C for 24 h without using conventional metal catalysts. Each insoluble phase is isolated from each primary hybrid product using dichloromethane (DCM) to selectively dissolve the soluble polymer phase.

X-ray diffraction (XRD) is used to verify the morphology of the insoluble phases. This demonstrates that the molecular sheets of the LDH-carbonate are fully dismantled during the polymerization. Porous, network morphology is established for some of the insoluble phase structures using scanning electron microscopy (SEM). This indicates potential suitability of these self-assembled insoluble phase materials as bioscaffolds for artificial cell growth. Nuclear magnetic resonance spectrometry (NMR) was used to determine the ratio of ester to acidic carbonyls in the insoluble phase. Energy dispersive X-ray spectroscopy was also used to determine the ratio of magnesium to aluminium in the insoluble phases.

Keywords

poly(lactide), caprolactone, valerolactone, layered double hydroxide, tissue scaffold, network.

1.0 **Introduction**

Tissue engineering has evolved greatly since the mid-1980s into a multidisciplinary field targeting the restoration, maintenance and improvement of tissue functions Fay et al. (2007), Langer & Vacanti (1993), Chen et al. (2009), Vaz et al. (2005), Vunjak-Novakovic et al. (2010), Operpenning et al. (1999), Schmidt & Leach (2003), Kuo et al. (2010). In particular, poly(lactic acid) (PLA) is a popular polyester material that is used in tissue engineering because of its excellent biocompatibility and mechanical properties. Good adherence and differentiation properties have been observed for osteoblasts cultured on PLA membranes, Santos et al. (2009), Liu et al. (2004). Similar to PLA, poly(ε-caprolactone) (PCL) and poly(δ-valerolactone) (PVL) are often employed for use in bio-scaffold applications. Their advantage in this application is their relatively low degradation rate (during hydrolysis in aqueous media). Therefore, they have been copolymerized with a variety of polymers including collagen, poly(glycolic acid), poly(lactic acid) and poly(ethylene oxide), Vroman & Tighzert (2009).

Layered double hydroxides (LDHs) comprise an unusual class of layered inorganic materials with positively charged layers and weakly bound, usually exchangeable, charge-balancing anions Manzi-Nshuti et al. (2009). LDHs have been studied and characterized by multiple researchers, e.g., Perez-Amaro et al. (2009), Swanson et al. (2013), Kang et al. (2004).

Ring-opening polymerization (ROP) has been proposed as the main mechanism by which a monomer can be ring-opened at the cation of an LDH sheet, and can then propagate to form a polymer chain anchored on this LDH sheet, McCarthy et al. (2013). Generally, ROP may occur by either cationic, anionic or coordination-insertion routes Kricheldorf (2001). In addition to ROP at the LDH sheet, a combination of polycondensation of ring-opened monomers and ROP by free ions in the polymer bulk may also occur.

63 In this paper, the formation of various insoluble polymer-based Mg poly(lactone) networks have
64 been demonstrated by polymerizing different lactone monomer combinations using LDH-
65 carbonate as an initiator for the first time; this is an approach, which avoids the use of any
66 potentially toxic conventional metal catalysts. There is also no long-chain acid intercalant present
67 in the LDH, as used previously (McCarthy et al. (2013)), which proves that the LDH itself is
68 sufficient to initiate polymerisation and network formation without the aid of a long chain
69 intercalant. Some of the insoluble network phases are potentially suitable for use as bioscaffolds
70 for cell growth, based on their porous morphology. The main advantage of this system over
71 established scaffold fabrication technologies is the capacity to tailor the chemistry of the resin
72 material using different monomer combinations and types of layered double hydroxide. The
73 scaffold is self-assembled at the molecular level and does not require specialised electrospinning
74 or other physical deposition technologies (e.g. chemical vapour deposition, photolithography, or
75 electron beam lithography, Prabhakaran (2012). This provides the potential to remove such
76 deposition steps from scaffold preparation, hence reducing cost. It also provides the potential to
77 modify the cations and intercalated species of the LDH-initiator to include beneficial active
78 ingredients for the cell growth process directly in the scaffold structure.

79 **2.0 Materials and Methods**

80 ε-caprolactone (97%) and δ-valerolactone (technical grade) were both obtained from Aldrich. ε-
81 caprolactone, which is liquid at room temperature, and δ-valerolactone were stored at 4 °C before
82 use. L,D-lactide (99%) was obtained from Alfa Aesar. All the three materials mentioned above
83 were used as monomers in the polymerization process. The initiator, synthetic layered double
84 hydroxide carbonate, was obtained from Aldrich. LDH-carbonate has a layered structure with a
85 high anionic exchange capacity that allows it to host and release various anionic compounds. Its

chemical formula is $Mg_6Al_2(CO_3).(OH)_{16}.4H_2O$. Since L,D-lactide and LDH-carbonate are both sensitive to moisture, it is essential to avoid their re-adsorption of water. Thus, when they were not being used immediately, they were both stored over a desiccant. L,D-lactide was sublimed immediately prior to reaction to remove moisture.

2.1 Sample Preparation

A schematic of the specimen preparation process is given in Figure 1. This comprised the polymerisation of a mixture of monomer(s) plus LDH followed by dissolution of the product in methylene chloride followed by centrifugation of the solution to result in an insoluble residue which was dried to result in two separate phases of the polymer, soluble (SOL) and insoluble (INSOL).

2.1.1 Reaction Set 1: Mixture of L,D-lactide and LDH-Carbonate

A mixture of L,D-lactide and LDH-carbonate was prepared in the ratio of 95:5 by mass. 5 g of the mixture was put into a 100 ml glass bottle, followed by intense mixing using a mechanical mixer (Vortex Genie obtained from VWR International). Since L,D-lactide sublimes at 125 °C, an aluminium foil was used to seal the vial and retain the subliming monomer at the reaction temperature (150 °C). The product of this reaction was labelled PLDLA-HYB (HYB = hybrid), while its soluble and insoluble phases were labelled PLDLA-SOL and PLDLA-INSOL, respectively.

2.1.2 **Reaction Set 2: Mixtures of L,D-lactide & ε-Caprolactone (LC) and L,D-lactide & δ-Valerolactone (LV) with LDH-Carbonate.**

The LDH-carbonate initiator comprised 5% by mass of each overall reaction mixture, while the monomer mixtures, L,D-lactide & ε-caprolactone (hereafter referred to as LC) and L,D-lactide & δ-valerolactone (hereafter referred to as LV) were mixed in the ratios of 1:2, 1:1, and 2:1,

respectively, by mass. The resulting products were LC1:2-HYB, LC1:1-HYB, LC2:1-HYB, LV1:2-HYB, LV1:1-HYB, and LV2:1-HYB.

2.1.3 Hybrid polymerization process

All the initial hybrid polymer products with different initial monomer ratios were synthesised at 150 °C for 24 h in a Heraeus Incubator oven. The 100 ml reaction vials were fully sealed by aluminium foil wrap at the top of each vial to prevent escape of monomer vapour at temperatures greater than 125 °C. A minimal headspace was allowed to ensure that the L,D-lactide vapour remained trapped in intimate contact with the reaction bulk.

Separation of each initial hybrid product into soluble (SOL) and insoluble (SOL) fractions by methylene chloride solvent extraction and centrifugation. Each initial hybrid product consisted of a soluble polymer, an insoluble polymer-salt complex phase and any residual monomers. Therefore, methylene chloride (dichloromethane (DCM)) (obtained from Fisher Chemicals) was used as a solvent to dissolve the soluble polymer phase so that the insoluble phase could be isolated. The extraction procedure was as follows: Once each reaction sample was cooled to room temperature, 60 ml DCM was added to the sample in a vial and the solution was mixed with a magnetic stirrer for 12 h (the concentration of the solution was about 0.083 g/ml). Once the hybrid was fully dissolved in the solvent, the solution was equally separated into four 15 ml centrifuge tubes that were placed in a centrifuge. The centrifuge (Sigma 4-16 centrifuge) was operated at a speed of 800 rpm or 10375 RCF (Relative Centrifuge Force), for 10 min. When the centrifugation was finished, the upper supernatant was gently poured off or removed by syringe, and the insoluble residue was allowed to dry fully at room temperature for 24 h. Then, the centrifuge tubes were placed in an oven at 50 °C for an hour to ensure complete removal of the methylene chloride (boiling point: 39 °C).

2.1.4 Characterisation Methods

The samples used for characterization studies were desiccated and finely powdered. Thermogravimetric analysis (TGA) was performed using a Perkin-Elmer/Seiko machine under a nitrogen atmosphere avoiding further oxidations. Isothermal thermogravimetry was performed by heating the well-mixed primary product after polymerization at 150 °C for 6 h with an initial heating rate of 20 K/min. Note that these isothermal TG measurements were unable to remove the δ-valerolactone and ε-caprolactone monomers, which both have higher boiling points (ε-caprolactone: 253 °C; δ-valerolactone: 260 °C). Therefore, at 150 °C, only the amount of residual L,D-lactide in each of the products could be calculated. Determination of ε-caprolactone and δ-valerolactone was subsequently made by conducting isothermal measurements on hybrid reaction products at 260 °C for 6 h. However, at 260 °C some decomposition of the respective polymers can also occur, which means that the residual ε-caprolactone and δ-valerolactone are likely overestimated. Then, initial primary product samples from the same batch were also heated by temperature-ramp to 600 °C at a heating rate of 10 K/min. An Al pan was used to hold samples. The typical sample masses for both procedures were 19 mg and 16 mg, respectively. The mass loss was measured in a N_2 atmosphere, with N_2 flowing at 100 ml/min to minimize the extent of any oxidation. The temperature, time and mass loss for each specimen were.

Scanning electron microscopy (SEM) was performed using a Philips XL30 FEGSEM. Prior to the SEM imaging, the samples were sputter-coated with Pt using a sputter-coater (Gatan Inc.) for 3 min. Typical SEM parameters were: Beam energy: 8 keV, rotation angle: 50°, rotation rate: 30 rpm.

153 The X-ray Diffraction (XRD) spectra were obtained on a Bruker D8-Advance spectrometer using
154 Kα radiation (λ = 0.154 nm) over a 2θ range of 2-70 ° with a scan rate of 0.50 °/min. The
155 uncertainty of the measurement was ±0.01 °. Prior to the test, the samples were ground to powder.
156 FTIR was used to obtain the FTIR absorption spectra using a Nicolet 5700 FTIR spectrometer. For
157 each sample, 32 scans were employed over a wavenumber range 400 cm^{-1} –4000 cm^{-1}.
158 ^{13}C Nuclear Magnetic Resonance (NMR) spectra of the extracted scaffold residues were obtained
159 using a Bruker Advance III 400 MHz spectrometer. The settings used were 1.36 seconds
160 acquisition time, 32768 points counted and 24038 Hz sweep width. 7200 Hz was selected as the
161 spin rate for the tests of all the insoluble scaffold solid powders so that a higher resolution of peaks
162 could be obtained within the shorter acquisition time. Adamantane was used as the standard
163 reference for tuning purposes.
164 EDX (Energy dispersive X-ray) analysis of scaffold samples was performed with a Philip XL30
165 FEGSEM scanning electron microscope equipped with an Rontec (now Bruker) energy dispersive
166 spectroscopy (EDS) analytical system (with a silicon drift diode detector). 0.05 g material samples
167 were pressed mechanically into a circular disc with 10 mm as the diameter. To quantify the
168 chemical content of areas with different area space (around 46000 μm^2) on the homogeneous
169 sample surface, distinctly different topographical areas ($N \geq 3$) were chosen from the sample and
170 examined at 10 kV using Quantax 400 (from Bruker) software.
171

3.0 **Results and Discussion**

3.1 Specimen Appearance

Photographs of a selection of the specimens are presented in Figure 2. Fig 2(a) shows PLDLA-HYB as produced, while Figure 2(b) shows a selection of the insoluble phase materials isolated from various hybrids as labelled. The latter specimens, especially PLDLA-INSOL, were fine fibrous materials that could be pressed into cohesive mats.

3.2 Thermogravimetric analysis (TGA)

Isothermal and ramp TGA were used to measure the residual solid mass yields (to derive polymer mass yields by calculation) of the various single- and multi-lactone/LDH polymer hybrid products, respectively. The polymer mass yields determined are shown in Figures 3 and 4.

3.2.1 Isothermal Thermogravimetric Analysis: Homopolymers.

In the polymer mass yield data, (Figure 3), the PLA and PCL homopolymer hybrids achieved above 87% polymer yield by mass but the PVL-HYB achieved a yield of only 48.5%. As δ-valerolactone does not vaporise at 150 °C, it cannot have accounted for the mass loss in this TG test. Thus, the monomer or its short chain PVL polymer derivatives may have decomposed into smaller straight chain products, which may have vaporised at 150 °C. The isothermal TG of PLDLA-HYB, polymerized under the same conditions, shows a high polymer yield of 87.3% by mass, which is slightly lower than the value of 88% by mass reported in the literature for stearate-intercalated LDH by McCarthy et al. (2013).

3.2.2 Isothermal Analysis: Copolymer Products.

Figure 4 shows isothermal TG data for samples that were synthesised from binary mixtures of either L,D-lactide and ε-caprolactone (LC hybrids) or L,D-lactide and δ-valerolactone (LV hybrids) with various monomer combination ratios. The polymer mass yields of some of these

copolymerization products were slightly higher than those of the single monomer-derived products (Fig. 3). Thus, ε-caprolactone may have polymerised more easily on initiation sites of the LDH in the presence of L,D-lactide as an enabling co-monomer. Since both the ε-caprolactone and δ-valerolactone molecules are larger than the L,D-lactide molecule, they may not diffuse into the LDH galleries as well as L,D-lactide. Hence, during the copolymerization, the LDH sheets may have been firstly partly expanded or dismantled by the L,D-lactide propagation, and then the other two monomers were better able to diffuse into the LDH structure and access the internal sheet reaction sites. For example, when δ-valerolactone was copolymerised with L,D-lactide in three ratios using LDH, (LV series) the isothermal polymer mass yields were significantly increased from 48.5% by mass (PVL) to above 84% by mass. The polymer mass yields (which are adjusted to account for the original 5% by mass LDH-carbonate in the original reaction mixtures) and insoluble fractions for the various hybrid products are shown in Table 1.

The key observation here is that the polymerisation of either ε-caprolactone or δ-valerolactone alone produces dramatically different results to that of l,d lactide polymerisation: For PCL-HYB, a relatively high polymer mass yield is produced, but the insoluble mass fraction is far lower (7.2% by mass), than those for either PLDLA-HYB or any of the copolymer products. For PVL-HYB, the insoluble fraction is similarly low (6.2% by mass), indicating that L,D-lactide is a key promoter of insoluble material formation and may even be essential to enable the formation of network phases to mass fractions of the order of 25 to 30% by mass.

3.3 Scanning Electron Microscopy

A range of SEM images (Figs. 5-8) were taken to show the microstructure of the materials at various magnifications. Materials shown are LDH-carbonate, (Fig 5a), the initial hybrid products, (Figs. 4b and 5) and the scaffolds that were extracted from various polymer products: i.e., PLDLA-

HYB (L,D-Lactide alone), the LC hybrids (L,D-lactide & ε-caprolactone) and the LV hybrids (L,D-lactide & δ-valerolactone), respectively, (Figs 7 & 8). In some insoluble phases of the above, the porous structure and morphology beneficial for use as a bioscaffold are clearly visible (e.g., PLDLA-INSOL, LC-INSOL 1:1, and LV-INSOL 1:2, Figure 7), while the insoluble phases of other products show no clear network formation (e.g., LC INSOL 1:1, LV INSOL 2:1, Fig. 8).

The porous structures of the network-forming insoluble phases are substantially heterogeneous in size and shape. For PLDLA-INSOL (Figure 7), a visible fibre-like structure can be seen extending in a three-dimensional network, and the thickness of each pore wall is approximately 30-60 nm. The highly hierarchical and heterogeneous structure of the material is also clearly visible. Two types of structure dominate: a) long fibrous strands of material (Fig. 7b), and b) shorter more crosslinked strands of materials forming three-dimensional networks with oblong pores of length approximating 500 nm (Fig. 7c). However, no visible network can be seen in either PCL-INSOL or PVL-INSOL (Fig. 6), and their morphologies show significant similarities to that of pristine LDH-carbonate, (Fig. 5a), which suggests that neither ε-caprolactone nor δ-valerolactone in isolation will form significant insoluble phase material with LDH-carbonate. (This conclusion is confirmed by the corresponding similarity of their respective X-ray diffraction spectra to that of LDH-carbonate, (Fig. 10e, below) where reflections due to the Mg-O and Al-O bonds at LDH sheet level remain substantially unaltered relative to the pristine LDH-carbonate, indicating little participation of the LDH-carbonate sheets as initiating sites). The PCL- and PVL-INSOL SEMs (Fig. 6) show relatively homogeneous structures consisting of microspheres, and PCL-INSOL is characterised by much smaller grain structure than PVL-INSOL. However, in both of the latter, there is an absence of the distinctive network morphology evident for PLDLA-INSOL in Fig. 7c. Thus, it is clear that the L,D-lactide monomer is a key component for production of network

morphology characteristic of many bioscaffold materials and that neither PCL-INSOL or PVL-INSOL could be deployed as scaffolds for many tissue types.

3.4 X-ray Diffraction

X-ray powder diffraction spectra for magnesium l,d-lactate hydrate, the nine insoluble fractions, and pristine LDH-carbonate are shown below in Figs. 9, 10A and 10B. The LDH-carbonate spectrum (Fig. 9(e)) is characterised by a first-order peak at 0.76 nm, which represents the interlayer d-spacing of the LDH-carbonate initiator. The second peak at 0.38 nm is associated with a non-basal reflection, which represents the distance between the two cations in the sheet (i.e., Mg^{2+} and Al^{3+}), Klawitter et al. (1976). The peaks in the region 35–45° represent the harmonic signals of the first-order peak. In the region 2θ = 50–70°, there are two visibly defined peaks at 0.152 and 0.149 nm. These are attributed to the bond distances of Mg-O and Al-O in the molecule structure, respectively Cochechi et al. (2010). In the PLDLA-INSOL spectra, a strong peak is found at around 0.92 nm and multiple other peaks occur in the range 0.46–0.41 nm. The most intense of these peaks correspond closely to those of the magnesium L,D-lactate reference spectrum. (i.e., those at 0.92 and 0.51 nm, respectively, which both correspond to peaks in the PLDLA-INSOL residue spectrum).

The spectra of PCL-INSOL and PVL-INSOL (Fig. 9c and 8d) show almost the same pattern as the spectrum of LDH-carbonate except for two peaks located at 0.4 nm and 0.31 nm. Moreover, none of the characteristic peaks of Mg l,d-lactate are observed in the two insoluble spectra.

This evidence indicates that the LDH-carbonate sheets remain essentially intact for PCL-INSOL and PVL-INSOL, so that it is assumed that only a few monomers have attached to the internal LDH-carbonate sheet initiation sites within the interlayer. This finding is in accordance with the

data found in TGA measurements (Table 1), which show very low insoluble mass fractions for both PCL-INSOL and PVL-INSOL. By contrast, the PLDLA-INSOL shows a completely different XRD spectrum to that of LDH-carbonate (Fig. 9b), demonstrating that LDH-carbonate has been fully reacted and dismantled during the polymerization of L,D lactide alone. Moreover, the PLDLA scaffold synthesised in this paper is morphologically similar to magnesium-lactate (one strong identical peak at 0.92 nm), and is similar in structure to the magnesium-lactate reported by McCarthy et al. (2014) [16] for L,D lactide polymerised with LDH-stearate.

The spectra of the other six copolymer-based scaffold residues, Figs. 10A and 10B, are considerably different compared with that of the LDH-carbonate, demonstrating that new species have been generated by the reaction in each case. However, it is clear that the Mg-O peaks in these copolymer spectra at 0.15 nm are substantially less intense compared with the equivalent peak in the LDH-carbonate spectrum, indicating that Mg is the dominant active cation consumed by polymerisation and salt formation. Consistent with this, a compound similar, but not identical to, magnesium lactate can be observed in the spectra of the insoluble species. However, it is clear that another salt most likely co-exists with the magnesium lactate. From literature crystallinity studies, evidence for the existence of magnesium/aluminium carbonate, and magnesium/aluminium oxides here can be excluded, Gunawan and Xu (2008), Cava et al. (2007). Therefore, the co-existent salts are most probably magnesium caprolactate and magnesium valerolactate, as there are no other feasible ester species. Insoluble species with magnesium lactate feature a higher degree of network formation, and porous, open, three dimensional networks tend to dominate over other morphologies (e.g. spherules), when Mg-lactate is present in the necessary concentration.

3.5 Fourier Transform Infrared Spectroscopy

The FTIR spectra of L,D-lactide, LDH-carbonate and various insoluble phases synthesised by different monomer combinations are shown in Fig. 11 and Fig. 12. The FTIR spectrum for L,D-lactide (Fig. 11(a)) depicts its characteristic absorption bands at 1752, 1249, 928, 648, and 476 cm^{-1}. Specifically, 1752 cm^{-1} represents the two carbonyl groups in the ring structure, while the peaks in the range 1249-928 cm^{-1} are attributed to $–CH_3$ and –CH groups, and the remaining peaks from 648 cm^{-1} downwards represent water molecules. In the FTIR spectrum of LDH-carbonate, the peak at 3412 cm^{-1} represents the –OH group, while the CO_3^{2-} group is assigned to the peak at 1361 cm^{-1}. The remaining peaks, which have wavenumbers lower than 770 cm^{-1}, are assigned to the water molecules in the LDH-carbonate interlayers in the pristine hydrotalcite (LDH).

The features observed in the PLDLA-INSOL spectrum include the main peaks at 1585 cm^{-1} (C=O), 1469 cm^{-1} (bending $-CH_3$) and 1121 cm^{-1} (stretch C-O) rather than the 1752 cm^{-1} (ring carbonyls) and 1249 cm^{-1} ($–CH_3$ and –CH groups) from the monomer or 1361 cm^{-1} (CO_3^{2-} group) from the LDH-carbonate, Al-Itry et al. (2012), Heraldy et al. (2016), which indicates a clear distinction between the insoluble phase and both of the latter species. This confirms that a substantial chemical reaction has taken place between L,D-lactide and LDH-carbonate. However, the spectrum of PLDLA-INSOL still shows broad peaks around 3338 and 553 cm^{-1}, which are attributed to hydroxyl groups coming from the initiator layer surface or interlayer water molecules in the system, Hussein et al. (2012).

The FTIR spectra of the co-monomer scaffolds, are quite similar to the PLDLA-INSOL spectrum. In particular, bimodal peaks around 1600 cm^{-1} are seen in spectra for LC 1:2 (Fig.11(c)) and LV 1:1 (Fig. 12(d)). It is notable that the dominant peak for LC 2:1 (Fig. 11(e)) is 1637 cm^{-1} with a 'shoulder' peak at 1593 cm^{-1}, whereas the latter peak is dominant for both LC 1:2-INSOL and LC

1:1-INSOL. The peak at 1637 cm^{-1} can be attributed to bicarbonate ions, Arihara et al. (2001), which could have been formed by the reaction of carbonate anions, water and atmospheric carbon dioxide absorbed into the initiator inner layer space. Examining the copolymer scaffold FTIR spectra, the peaks at 1585, 1121, and 553 cm^{-1} are not as intense as those in the PLDLA-INSOL spectrum; therefore, it is possible that PLDLA-INSOL has the most pronounced crystallinity of all the scaffolds (See He et al. (2000) for a discussion of the application of FTIR to studying crystallinity of a lactone polymer).

The main conclusion from these results is a) the complete dissimilarity of spectra for insoluble species to that of the LDH initiator, b) the close similarity (but not identity) of spectra for all copolymer species to that of PLDLA-INSOL, which indicates that poly(lactide) is the dominant species in the insoluble phases, and that the ε-caprolactone and δ-valerolactone monomers play a negligible role in the formation of the insoluble phases.

3.6 Solid ^{13}C nuclear magnetic resonance spectroscopy

Figure 13 depicts the solid-state ^{13}C NMR spectra of the LC insoluble residues. It also features the spectra of magnesium lactate hydrate, Fig. 13(2), and the original LDH-carbonate initiator, Fig. 13(1). Generally, three main peak-types can be observed in the spectra shown below, which represent the methylene (19–33 ppm), methine (68 ppm), and carboxyl (170–183 ppm) groups, respectively.

In Fig. 13(1) (and Fig. 14(1)), the NMR spectrum for the LDH-carbonate initiator is shown. Clearly, the majority of its characteristic peaks cannot be observed in the spectra of any of the insoluble moieties. However, the LDH spectrum has one peak (169.5 ppm) very close to a peak of the PLDLA-INSOL spectrum (168.4 ppm) which could be attributed to the carbonyl bond of the

carbonate groups in both species. Nevertheless, the lack of all the other intrinsic LDH peaks in the INSOL spectra, clearly demonstrates that the characteristic layered structure of the LDH has been dismantled to beneath detectable limits during the polymerizations.

In Figs. 13(2), (and Fig. 14(2)), the reference spectrum for magnesium lactate is shown, while in Fig 12(3), the spectrum indicates the presence of PLDLA in the insoluble PLDLA-INSOL phase, which has characteristic signals at 16.7, 69.0, and 169.4 ppm, respectively, Saito et al. (2006). In the figure, the methine resonance can be seen at 68.2 ppm, and two ester-carbonyl signals can also be observed at 180.9 and 183.6 ppm (Fig. 13(2)) while ester peaks at 180.9 and 182.9 ppm also show the presence of a magnesium polylactone ester in addition to polymer moieties (e.g., an acid carbonyl at 177 ppm). In the LC series (Fig. 13(4)-(6)), the signals 24.2, 28.0, and 32.5 ppm indicate the incorporation of ε-caprolactone moieties in the copolymer. Likewise, in the LV series (especially Fig. 14(6)), the signals 27.7 ppm and 32.5 ppm are characteristic of δ-valerolactone shifts. Magnesium lactate or other polylactone ester moieties are detectable in the scaffold spectra for the LC and LV copolymer series at 180 and 183 ppm, respectively (Figs 13(4-6) and Fig 14(4-6)). The inorganic fraction of ester carbonyls in each insoluble species was determined by calculating the peak integrals of the carbonyl groups of the polymer (acid carbonyls) and ester moieties (ester carbonyls), respectively, as shown in Table 2.

This data indicates that no clear relationship exists between the initial monomer ratio and ultimate ester carbonyl yield in the insoluble phase. This would suggest that the ester carbonyl yield is driven by another factor, namely the number of Mg cations available to form ester moieties, which is primarily driven by the ratio of available LDH to monomer(s) in the reaction mixture.

Table 2 also shows the relevant calculated fraction of Mg in the original reaction mixtures, as well as the corresponding fractions of ester carbonyl functions measured by NMR on an INSOL and

353 HYB basis, respectively. It is clear that there would be insufficient Mg or Al to account for all of
354 the ester moieties detected in the insoluble phases, if one assumed the formation of Mg or Al *mono*-
355 lactate salts only (e.g., bonding of Mg with two single lactic acid monomers). Thus, in the absence
356 of non-metal ester-forming moieties, it is clear that only Mg or Al polylactone ester chains could
357 have formed (e.g., a Mg cation bonding to two polylactone chains to form a Mg polylactone ester).
358 Furthermore, based on Xray diffraction (XRD) evidence presented above, and previously, [1], Al
359 polylactone ester moieties are not detectable in INSOL to any significant degree, so that only Mg
360 polylactone ester moieties are considered in this discussion. (Specifically, it was shown by
361 McCarthy et al. [16] that a Mg:Al element ratio of 11:1 existed in the INSOL phase).

362 Overall, these NMR spectra demonstrate the formation of salt moieties in the insoluble phases, the
363 concurrent disassembly of LDH-carbonate initiator, and the ratio of ester to acidic carbonyl groups
364 in these phases, which can be used to calculate the proportion of ester species in each insoluble
365 phase. They fundamentally show the initiating activity of the LDH and its consumption to form a
366 chemically different insoluble species during the polymerisation process.

367 **3.7 EDAX (Energy-dispersive X-ray spectroscopy): Elemental Analysis of Reaction Species**
368 **and Products**

369 To complement the NMR analysis in Table 2, elemental analysis of the LDH-carbonate and the
370 insoluble phases was conducted to determine the magnesium and aluminium content in the two
371 polymer phases and to establish whether there was a fixed ratio of cations to ester groups in the
372 insoluble phases which would indicate the mechanism of insoluble phase ester formation. The
373 EDAX spectra are given in Figure 15, while Table 3 gives the corresponding elemental mass
374 fractions as calculated from these spectra by taking the ratios of the areas under the relevant

element peaks. One advantage of this measurement is its ability to confirm the local mass ratios of Mg to Al in each of the INSOL products and compare them with the original available fractions in the LDH-carbonate initiator. Doing this, it can be seen that an initial ratio of Mg:Al = 1.98 is measured in the LDH-carbonate initiator. This contrasts dramatically with almost complete selectivity of the pure poly(L,d-lactide) system for Mg in the PLDLA-INSOL insoluble phase (Mg/Al = 20.2).However, this trend is not observed for any of the copolymer INSOL phases, which all show Mg/Al ratios of the same order as that in the LDH-carbonate initiator (Mg/Al ~ 2). This would imply significantly different polylactone ester formation mechanisms as Mg and Al vary in valence, i.e., Mg^{2+} cations can form bidentate polylactone esters, whereas Al^{3+} cations can form tridentate esters. Clearly, the different molecular structures of these poly(lactone) ester networks could have an effect on the ultimate morphology of the insoluble phase network at the microscale, and may indeed account for the different morphologies of the different copolymer insoluble phase networks compared with that of PLDLA-INSOL.

Conclusions

In the current work, melt copolymerizations of various lactone monomer combinations of L,D-lactide, caprolactone and valerolactone have been performed for the first time using LDH-carbonate as an initiator. This process results in the formation of a novel embedded network in each two-phase polymer product, and the layered double hydroxide initiator undergoes near complete disintegration at the molecular level instead of intercalation or exfoliation. The mechanisms of the synthesis are believed to be predominantly anionic ring-opening polymerization and co-ordination-insertion polymerization (at the edges and faces of the LDH-carbonate sheets). Two phases, soluble and insoluble, were derived from all primary polymer products (hybrids) using dichloromethane (DCM, CH_2Cl_2) as extraction solvent. Some of these

398 CH_2Cl_2-insoluble phases, which have three-dimensional porous morphology at the microscopic
399 scale, can possibly be used as potential bio-scaffolds for cell growth.

400 The polymer mass yields of the nine hybrid products and their insoluble mass fractions have
401 been established by TGA and gravimetric analysis, while the microstructures and morphologies of
402 the pristine reactants, the initial hybrid polymer products, and the extracted scaffold residues have
403 been established using Xray diffraction (XRD) and scanning electron microscopy (SEM). In
404 general, the pores of all scaffolds produced are heterogeneously distributed (both spatially, and in
405 terms of pore size), and the morphologies are strongly dependent on the type and relative content
406 of monomers in the hybrid polymer-ionomer systems.

407 X-ray diffraction data demonstrated that LDH-carbonate sheets were almost fully dismantled
408 during the 24 h of polymerization in all the compositions except for the neat PCL- and PVL-
409 Hybrids. (PCL-HYB, PVL-HYB), where there was no network formation. This suggests that L,D-
410 lactide is a beneficial reaction component for maximisation of overall polymer yield and maximal
411 yield of insoluble scaffold material in these reaction mixtures.

412 This work confirms that carbonate-intercalated LDH-carbonate, the most common commercial
413 synthetic layered double hydroxide, is a viable initiator for the polymerisation of various lactone
414 homo- and copolymers to high polymer yields. It shows that a long chain acid intercalant species
415 is not essential to the polymerisation process. It is also possible to generate various embedded,
416 organically-insoluble networks with different morphologies that can be customised using different
417 comonomer types and combinations. Moreover, if required, the structure of the layered double
418 hydroxide used can be altered by chemical design to vary the cation and anion content in the
419 scaffold according to the specific requirements of a bio-scaffold application, for example. This is
420 something not possible with current physical deposition techniques, which also currently comprise

additional fabrication cost. It is expected that these materials can be used in a variety of scaffold applications and work continues to validate their performance.

Acknowledgements: The authors would like to thank Dr. Louise Carney, School of Materials, University of Manchester, for her help and assistance throughout the project.

Funding Sources: This research did not receive any specific grant from funding agencies in the public, commercial, or not-for-profit sectors.

References

Abe H., Thermal degradation of environmentally degradable poly(hydroxyalkanoic acid)s. 2006. Macromol. Biosci., 6, 469.

Al-Itry R., Lamnawar K., and Maazouz A., 2012 “Improvement of thermal stability, rheological and mechanical properties of PLA, PBAT and their blends by reactive extrusion with functionalized epoxy,” Polym. Degrad. Stab., 97, 1898–1914,.

Arihara K., Kitamura F., Ohsaka T., and Tokuda K., 2001 “Characterization of the adsorption state of carbonate ions at the Au(111) electrode surface using in situ IRAS,” J. Electroanal. Chem., 510, 128–135.

Baer T., Hase W.L., eds., 1996, Unimolecular Reaction Dynamics : Theory and Experiments: Theory and Experiments. Oxford University Press, USA.

Baimark Y. and Molloy R., Synthesis and characterization of a random terpolymer of L-lactide, ϵ-caprolactone and glycolide. 2004. Sci. Asia, 30, 327.

Bose, S.; Vahabzadeh, S.; Bandyopadhyay, A., 2013. Bone tissue engineering using 3D printing. Materials Today, 16, 497-513.

Cava, S.; Tebcherani, S. M.; Souza, I.; Pianaro, S.; Paskocimas, C.; Longo, E.; Varela, J., 2007. Structural characterization of phase transition of Al_2O_3 nanopowders obtained by polymeric precursor method. Mater. Chem. Phys., 103, 394-399.

Chen, M.; Przyborowski, M.; Berthiaume, F.; 2009. Stem cells for skin tissue engineering and wound healing. Crit. Rev. Biomed. Eng., 37, 399-421.

Cocheci L., Barvinschi P., Pode R., Popovici E., and Seftel E., 2010, Chem. Bull. Politehnica. Univ. Timisoara, 40, 55.

Faÿ F.; Renard E.; Langlois V.; Linossier, I; Vallée-Rehel K., 2007. Development of poly(ε-caprolactone-co-l-lactide) and poly(ε-caprolactone-co-δ-valerolactone) as new degradable binder used for antifouling paint. Eur. Polym. J., 43, 4800-4813.

Fernández J., Etxeberria A., and Sarasua J.-R., 2012. J. Mech. Behav. Biomed. Mater., 9, 100.

Gunawan, P.; Xu R.; 2008. Direct control of drug release behavior from layered double hydroxides through particle interactions. J. Pharm. Sci., 97, 4367-4378.

He Y. and Inoue Y., 2000 "Novel FTIR method for determining the crystallinity of poly(ε-caprolactone)," Polym. Int., 49, 623–626.

Heraldy E., Nugrahaningtyas K. D., Sanjaya F. B., Darojat A. A., Handayani D. S., Hidayat Y., 2016 "Effect of reaction time and (Ca+Mg)/Al molar ratios on crystallinity of Ca-Mg-Al layered double Hydroxide," IOP Conf. Ser. Mater. Sci. Eng., 107, 1, 012025.

Hulbert, S. F.; Young, F. A.; Mathews, R. S.; Klawitter, J. J.; Talbert, C. D.; Stelling, F. H., J. 1970. Potential of ceramic materials as permanently implantable skeletal prostheses. Biomed. Mater. Res., 4, 433-456.

Hussein S. H., Ali Al, Al-Qubaisi M., Hussein M. Z., Ismail M., Zainal Z., and Hakim M. N., 2012 "Comparative study of Mg/Al- and Zn/Al-layered double hydroxide-perindopril erbumine nanocomposites for inhibition of angiotensin-converting enzyme.," Int. J. Nanomedicine, 7, 4251–62.

Jeong, C. G.; Zhang H.; S. J. Hollister, 2011. Three-dimensional poly(1,8-octanediol-co-citrate) scaffold pore shape and permeability effects on sub-cutaneous in vivo chondrogenesis using primary chondrocytes. Acta Biomater., 7, 505-514.

Kang, M. R.; Lim, H. M.; Lee, S. C.; Lee, S.-H.; Kim, K. J.; 2004. Layered double hydroxide and its anion exchange capacity. Adv. Technol. Mater. Mater. Process. J., 6, 218-223.

473 Klawitter, J. J.; Bagwell, J. G.; Weinstein, A. M.; Sauer, B. W., 1976. An evaluation of bone
474 growth into porous high density polyethylene. J. Biomed. Mater. Res., 10, 311-323.
475 Kricheldorf, H. R.; 2001. Syntheses and application of polylactides, Chemosphere, 43, 49–54.
476 Kuo, C. K.; Marturano, J. E.; Tuan, R. S.; 2010, Sports Med. Arthrosc. Rehabil. Ther. Technol.,
477 2, 20.
478 Langer, R.; Vacanti, J. P. 1993. Tissue Engineering Science. 260, 920-926.
479 Liu, H. C.; Lee, I. C.; Wang J. H.; Yang, S. H.; Young, T. H., 2004. Preparation of PLLA
480 membranes with different morphologies for culture of MG-63 Cells. Biomaterials, 25, 4047-4056.
481 Ma, P. X.; Choi, J. W., 2001. Biodegradable polymer scaffolds with well-defined interconnected
482 spherical pore network. Tissue Eng., 7, 23-33.
483 Manzi-Nshuti, C.; Zhu, L.; Nyambo, C.; Wang, L.; Wilkie, C.A.; Hossenlopp J. M., 2009. Fire
484 and Polymers V, 1013. Washington, DC: American Chemical Society.
485 McCarthy, E. D.; Zammarano, M.; Fox, D. M.; Nieuwendaal, R. C.; Kim, Y. S.; Maupin, P. H.;
486 Trulove P. C.; Gilman J. W., 2013. Formation of extended ionomeric network by bulk
487 polymerization of l,d-lactide with layered-double-hydroxide. Polym., 54, 90-101.
488 Nanaki, S. G.; Pantopoulos, K.; Bikiaris, D. N.; 2011. Synthesis of biocompatible poly(ε-
489 caprolactone)-block-poly(propylene adipate) copolymers appropriate for drug nanoencapsulation
490 in the form of core-shell nanoparticles. Int. J. Nanomedicine, 6, 2981.
491 Oberpenning, F.; Meng, J.; Yoo J. J.; Atala A., 1999. De novo reconstitution of a functional
492 mammalian urinary bladder by tissue engineering, Nat. Biotechnol., 17, 149-155.
493 Pérez Amaro, L.; Coiai, S.; Conzatti, L.; Manariti, A.; Ciardelli, F.; Passaglia, E.; 2013. The effect
494 of layered double hydroxides dispersion on thermal and mechanical properties of poly(vinyl
495 chloride)/poly(methyl methacrylate) blends. Polym. Int., 62, 554-565.

Prabhakaran, M.P.; Venugopal, J.; Ghasemi-Mobarakeh, L.; Kai, D.; Jin, G.; Ramakrishna, S. 2012. In Biomedical applications of polymeric nanofibers, eds. R. Jayakumar, S. Nair, Springer, Berlin; Vol 2, p 21.

Saitô, H.; Ando, I.; Naito A.; 2006. Solid State NMR Spectroscopy for Biopolymers: Principles and Applications. Springer Science & Business Media.

Santos Jr, A. R.; Barbanti, S. H.; de R. Duek, E. A.; Wada, M. L. F., 2009. Analysis of the growth pattern of Vero cells cultured on dense and porous poly (L-Lactic Acid) scaffolds, Mater. Res., 12, 257-263.

Schmidt, C. E.; Leach J. B.; 2003. Neural tissue engineering: strategies for repair and regeneration. Annu. Rev. Biomed. Eng., 5, 293-347.

Swanson, C. H., Stimpfling, T.; Troutier-Thulliez, L.; Hintze-Bruening, H.; Leroux, F. 2013 Layered double hydroxide platelets exfoliation into a water-based polyester. J. Appl. Polym. Sci., 128, 2954-2960.

Vaz, C. M.; van Tuijl S.; Bouten, C. V. C.; Baaijens F. P. T., 2005. Design of scaffolds for blood vessel tissue engineering using a multi-layering electrospinning technique. Acta Biomater., 1, 575-582.

Vroman, I.; Tighzert, L., 2009. Biodegradable Polymers. Materials, 2, 307-344.

Vunjak-Novakovic, G.; Tandon N.; Godier, A.; Maidhof, R.; Marsano, A.; Martens, T. P.; Radisic, M., 2010, Challenges in cardiac tissue engineering., Tissue Eng. Part B. Rev., 16, 169-187.

519 # FIGURES

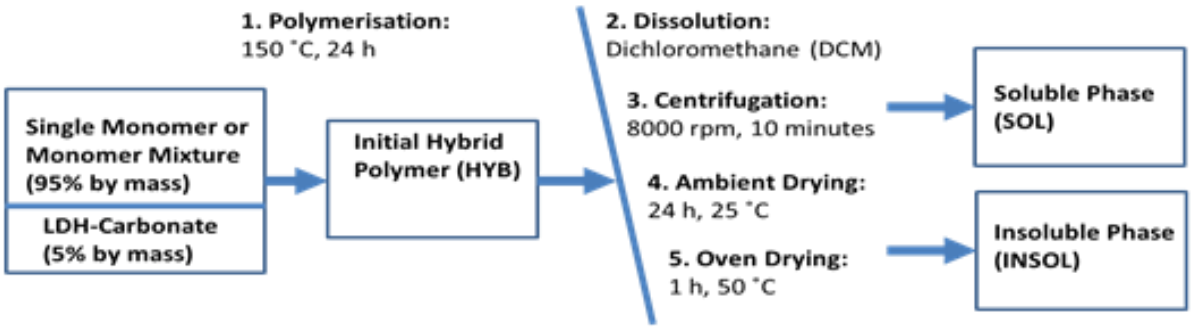

520

521 **Figure 1. Process schematic for polymerization of various products and their extraction with**

522 **methylene chloride to form scaffolds.**

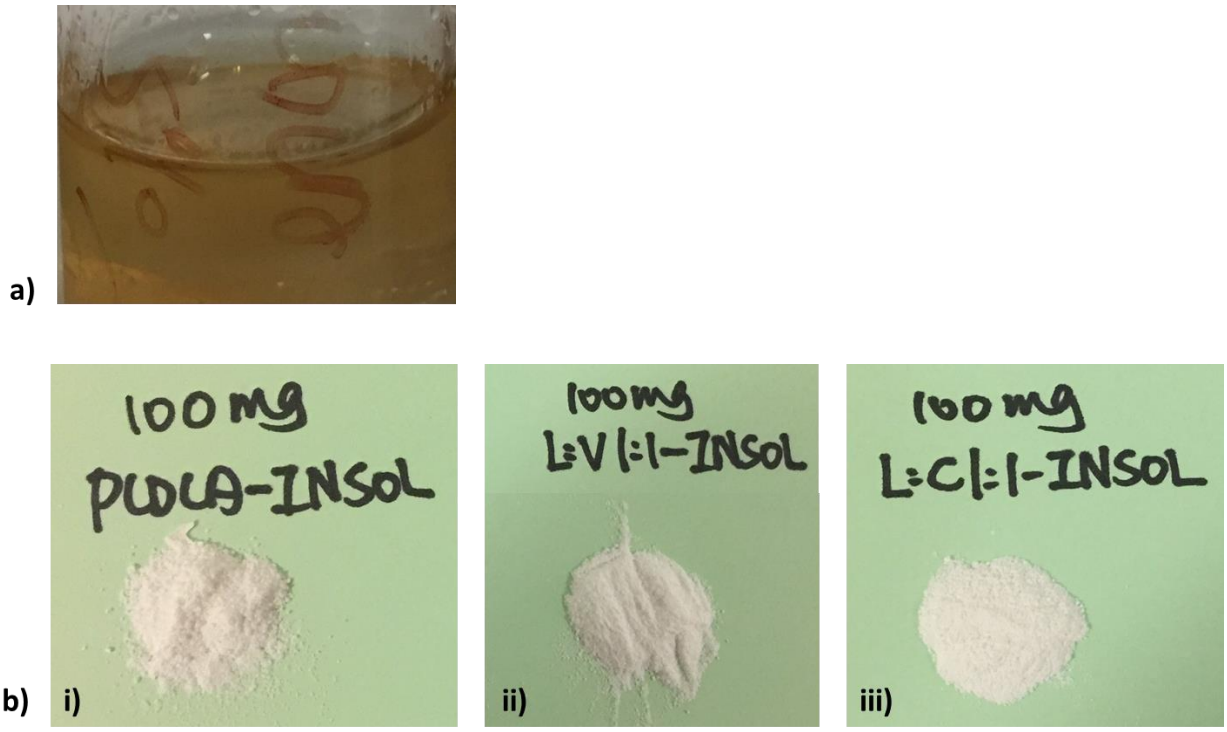

524

525 **Figure 2. Photographs of selected specimens produced: a) PLDLA-HYB resin specimen**

526 **(semi-transparent) b) selection of insoluble phase materials after extraction of soluble**

527 **phases: i) PLDLA-INSOL, ii) LV-1:1-INSOL, iii) LC-1:1-INSOL**

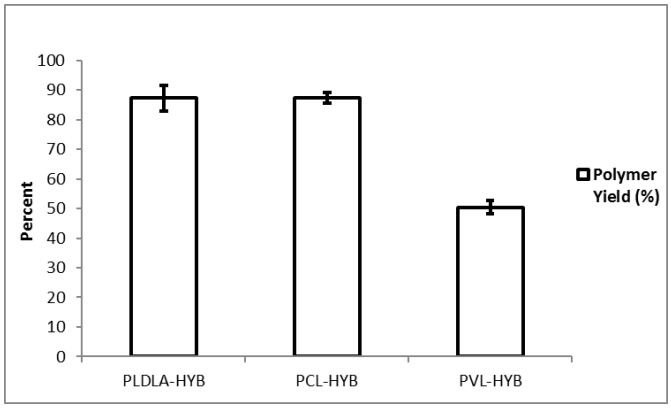

528

529 **Figure 3. Polymer mass yields of initial homopolymer hybrids determined by heating at 150**

530 **°C isothermally for 6 h (n = 3). Error bars = standard deviation.**

531

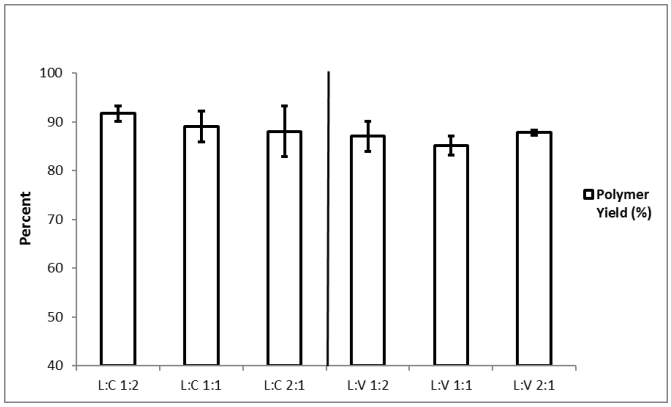

Figure 4. Polymer mass yields of hybrid products synthesised by different monomer combinations determined by heating at 150 °C isothermally for 6 h. (n = 3) Error bars = standard deviation.

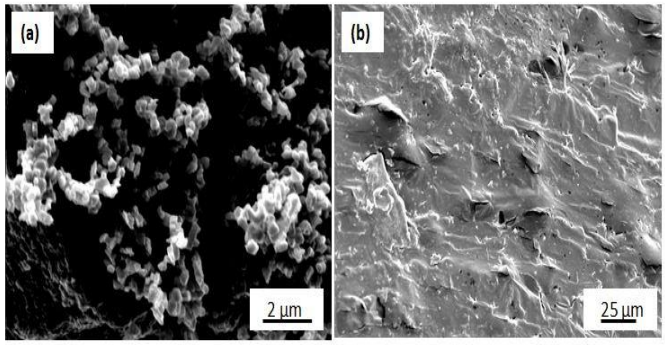

Figure 5. SEMs of (a) LDH-carbonate and (b) PLDLA-HYB at magnifications of 10,000 and 1,000, respectively.

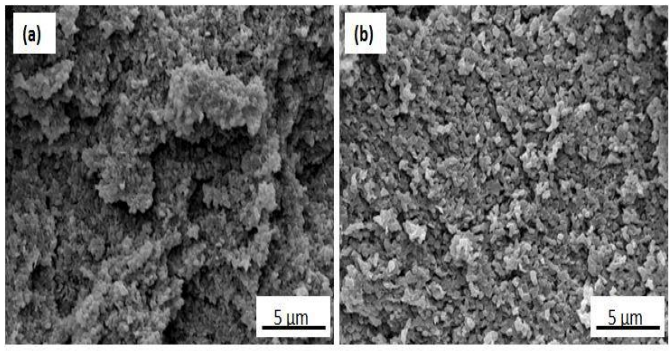

Figure 6. SEMs of (a) PCL-INSOL and (b) PVL-INSOL at magnification of 5,000.

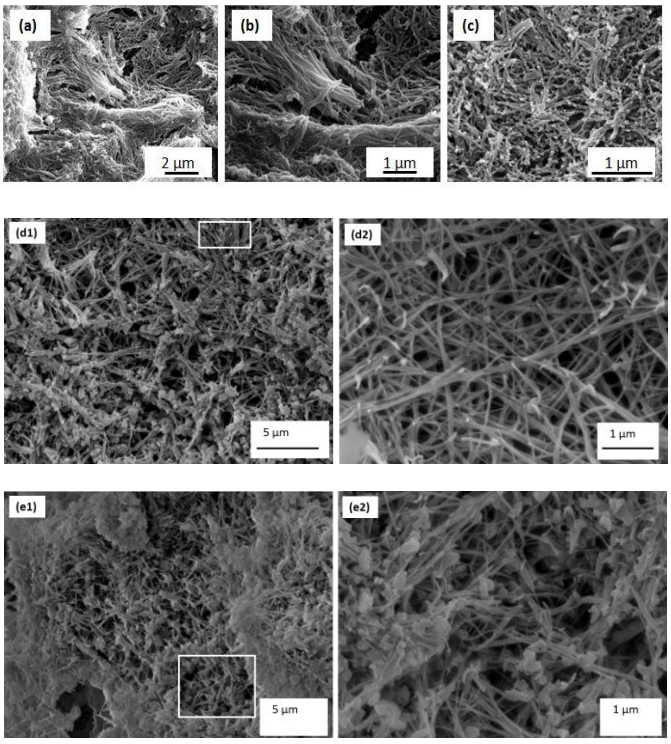

Figure 7. SEMs of good network formers: PLDLA-INSOL at magnification of a) 5,000, b) 12,500 and c) 40,000, (d1, d2) LC INSOL 1:2, and (e1, e2) LV INSOL 1:2.

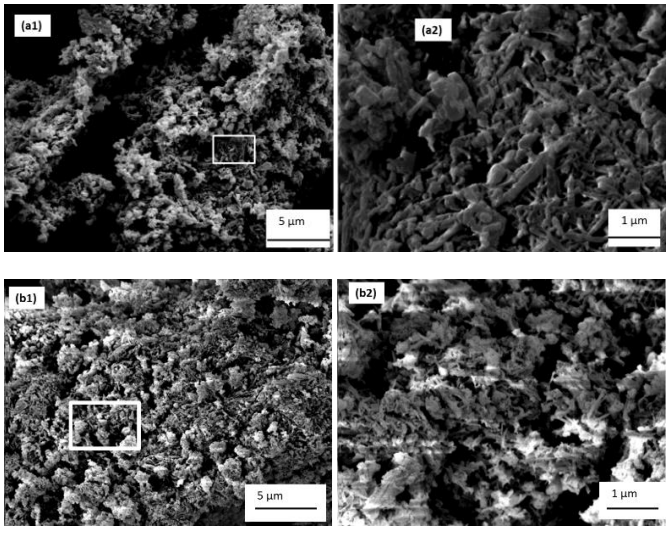

Figure 8. SEMs of non-network formers: a) LC INSOL 1:1 and b) LV INSOL 2:1.

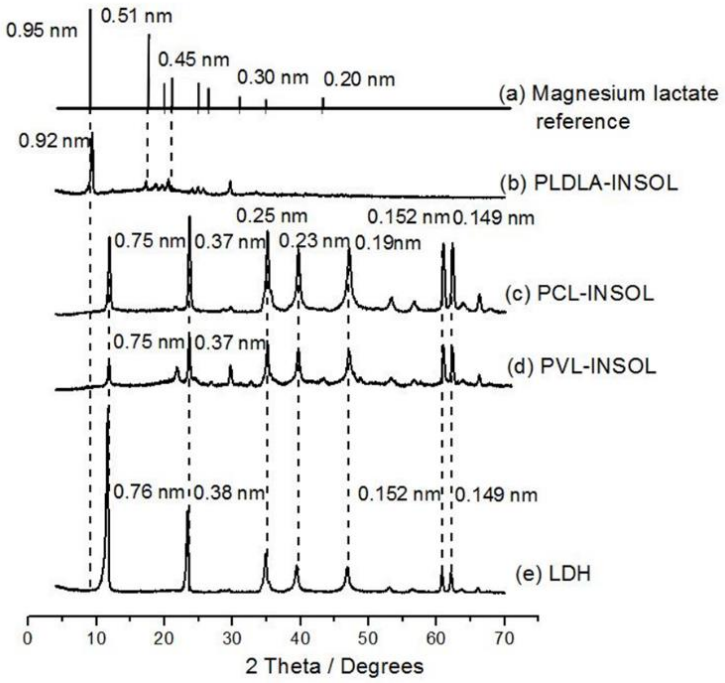

549

550 **Figure 9. XRD Spectra for scaffold residue synthesised by (a) magnesium l,d-lactate hydrate,**

551 **(b) PLDLA-INSOL, (c) PCL-INSOL, (d) PVL-INSOL and (e) pristine LDH-carbonate.**

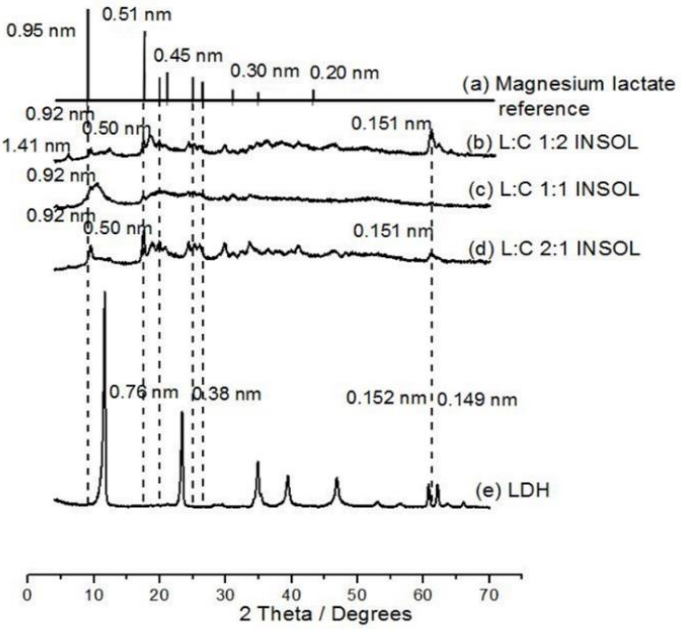

552

553 **Figure 10A. XRD spectra for scaffold residue synthesised using l,d-lactide and ε-**

554 **caprolactone monomers at different ratios.**

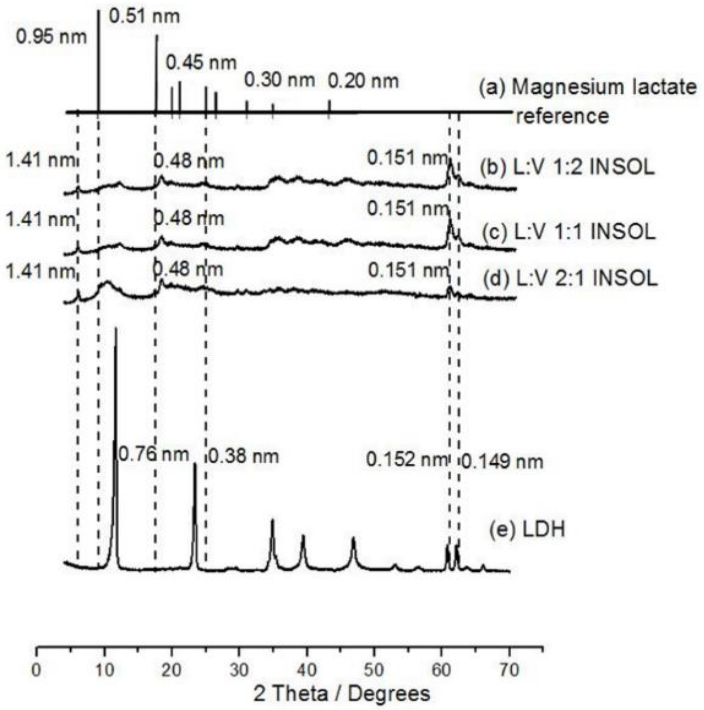

555

556 **Figure 10B. XRD spectra for scaffold residue synthesised using l,d-lactide and δ-**

557 **valerolactone monomers at different ratios.**

558

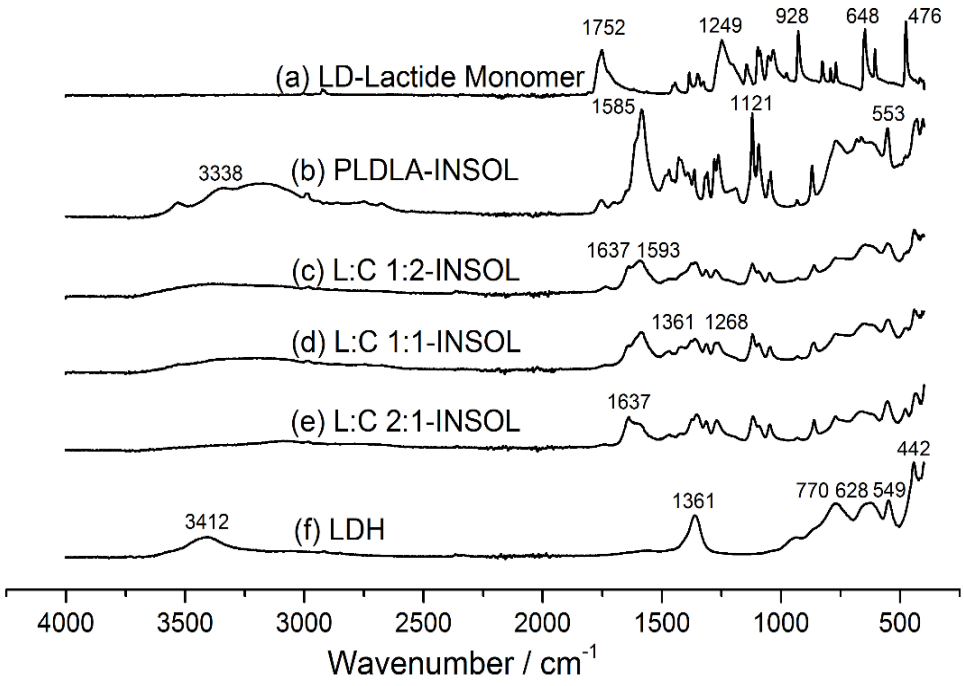

559

560 **Figure 11. Fourier transform infrared spectra of (a) L,D-Lactide monomer, (b) PLDLA-**

561 **INSOL and LC-INSOL series polymerised with L:C mass ratios of (c) 1:2, (d) 1:1, (e) 2:1**

562 **and (f) LDH-carbonate initiator.**

563

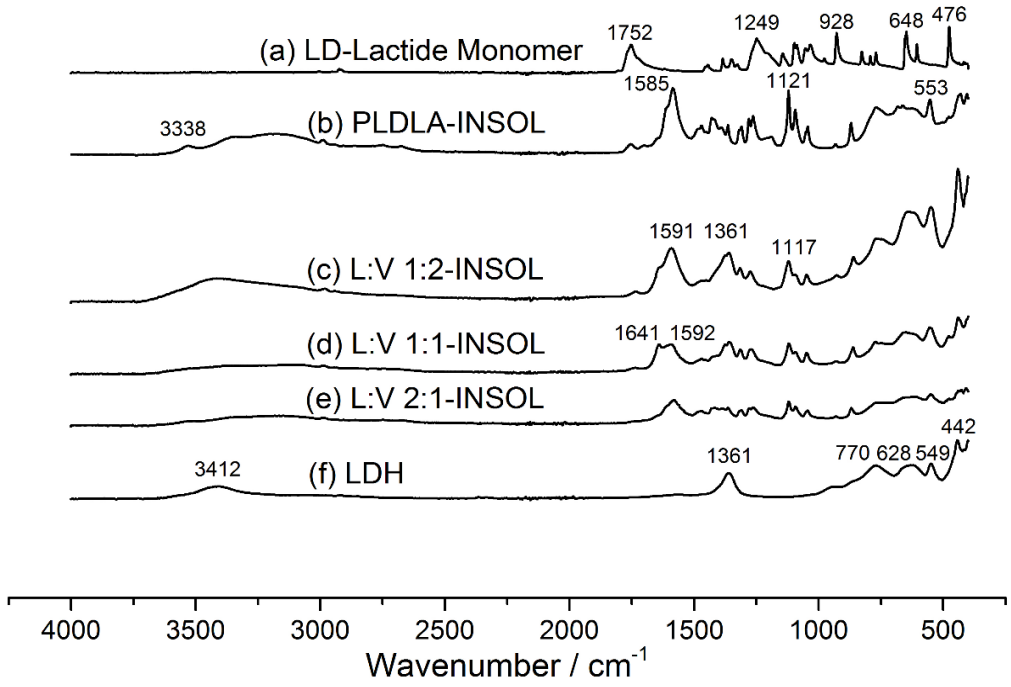

564

565 **Figure 12. Fourier transform infrared spectra of (a) LD-Lactide monomer, (b) PLDLA-**

566 **INSOL, the LV-INSOL series synthesised with L:V mass ratios of (c) 1:2, (d) 1:1, (e) 2:1**

567 **and (f) LDH-carbonate.**

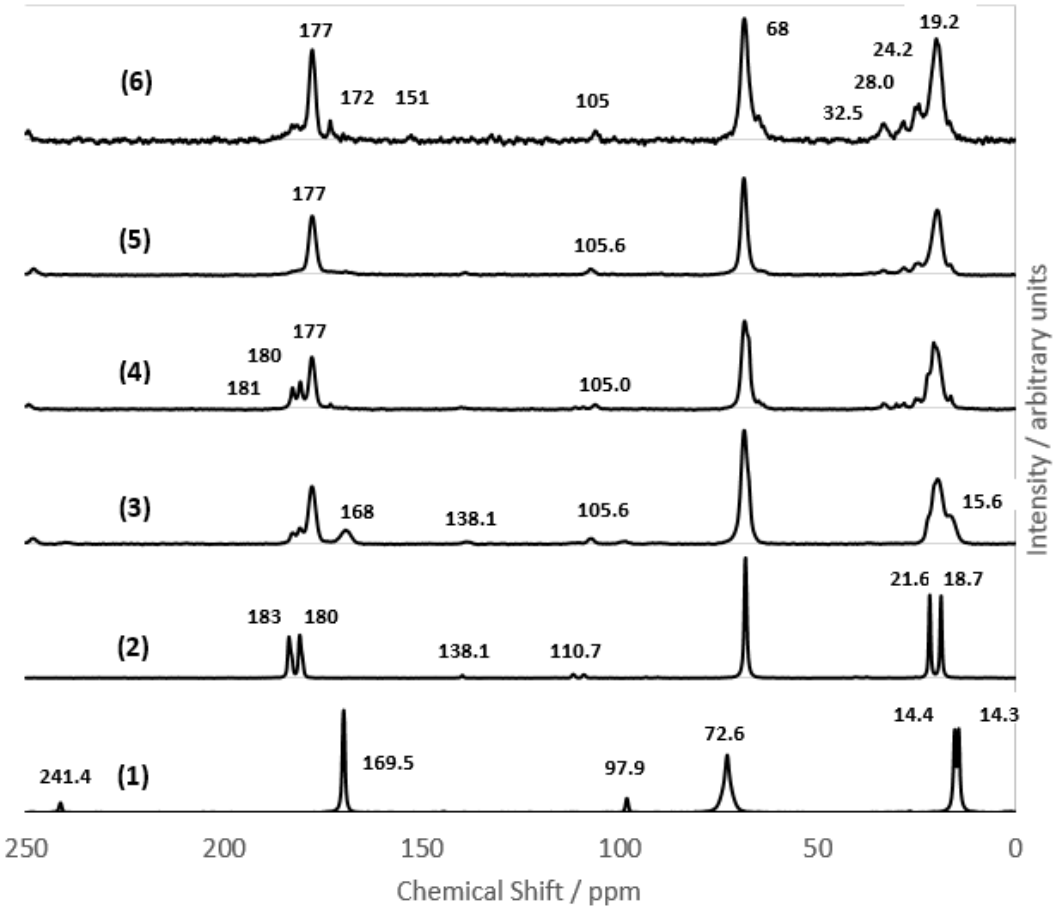

568

569 **Figure 13. Solid State ^{13}C NMR of various species in the reaction systems: (1) LDH, (2)**

570 **magnesium l-lactate hydrate, (3) PLDLA-INSOL, (4) LC 2:1 INSOL, (5) LC 1:1 INSOL, (6)**

571 **LC 1:2 INSOL, in the range 250-0 ppm.**

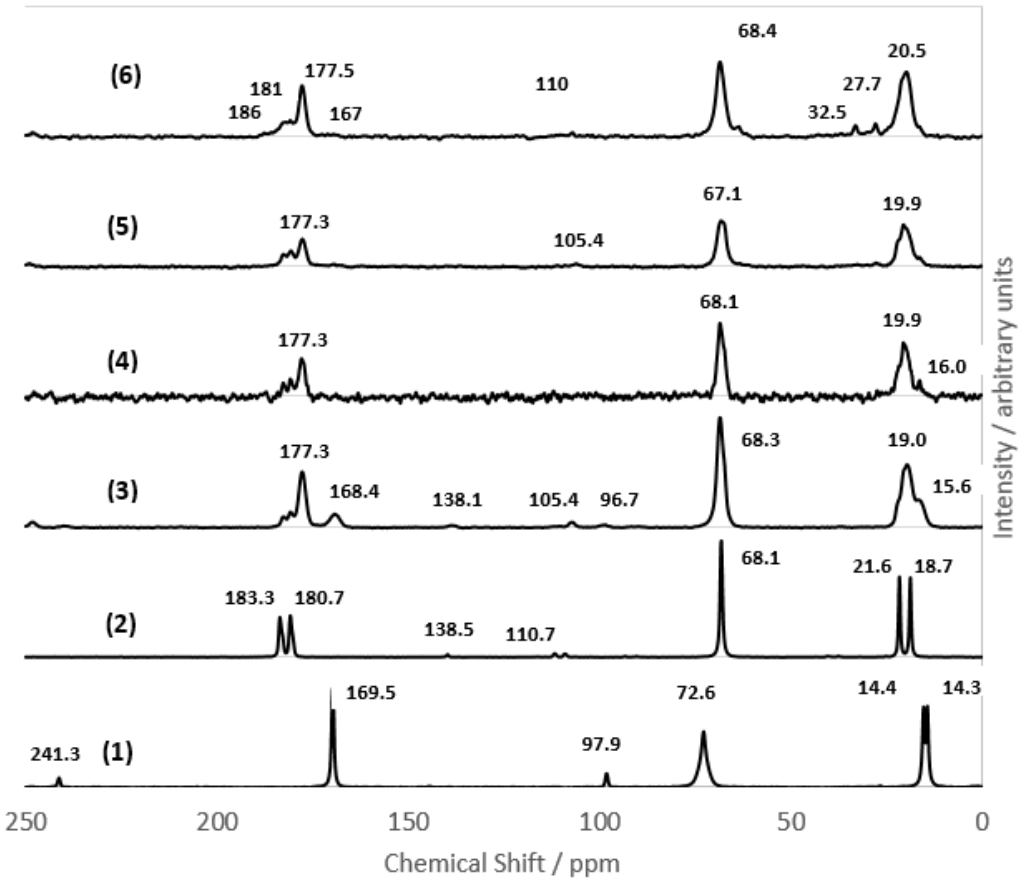

572

573 **Figure 14. Solid State ^{13}C NMR of various species in the reaction systems: (1) LDH, (2)**

574 **magnesium l-lactate hydrate, (3) PLDLA-INSOL, (3) LV 2:1 INSOL, (4) LV 1:1 INSOL, (5)**

575 **LV 1:2 INSOL, (6) LV 2:1 INSOL in the range 250-0 ppm, respectively.**

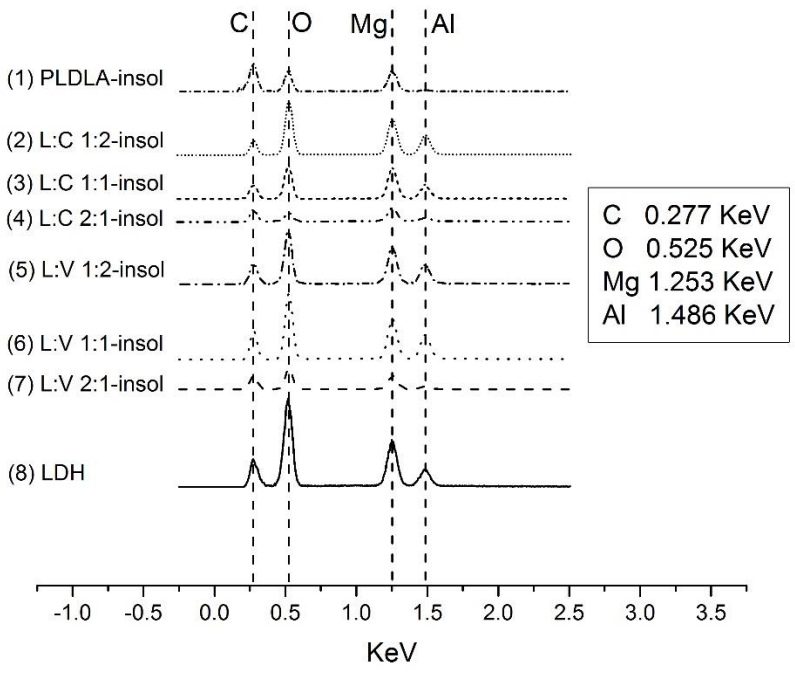

576

577 **Figure 15. EDAX Spectra of the various insoluble phases and LDH-carbonate.**

578

579

TABLES

Table 1. Overall polymer mass yields obtained from TGA and insoluble residue mass yields in the polymer hybrids with various monomer combinations. (n = number or runs).

Name	Polymer Mass Yield 150°C, 6 h (isothermal) (n = 3)	Mean Value at 260°C (ramp-TG) (n = 2)	Difference (on mean basis)	Insoluble Mass Fraction (Standard Deviation)
	% by mass			% by mass
PLDLA-HYB	87.3 (±4.3)	83.1	-4.2%	21.9 (±7.1)
PCL-HYB	87.4 (±1.9)	85.6	-1.8%	7.2 (±0.3)
PVL-HYB	48.5 (±2.3)	46.3	-2.2%	6.2 (±0.3)
L:C 1:2-HYB	91.7 (±1.5)	90.9	-0.8%	23.1 (±4.6)
L:C 1:1-HYB	90.8 (±3.1)	90.1	-0.7%	23.3 (±5.4)
L:C 2:1-HYB	88.1 (±5.3)	86.4	-1.7%	23.2 (±6.0)
L:V 1:2-HYB	87.1 (±3.1)	86.0	-1.1%	21.0 (±4.1)
L:V 1:1-HYB	86.7 (±2.0)	86.3	-0.4%	22.5 (±4.7)
L:V 2:1-HYB	87.8 (±0.2)	85.3	-2.5%	22.8 (±5.4)

585 **Table 2. Ester carbonyl mole fraction in the insoluble phases (INSOL) extracted from**
586 **different homopolymer and copolymer primary products (HYB).**

Name	Original Mg ion mole fraction, (HYB basis) (%)	Ester carbonyl mole fraction (INSOL Phase) (%)	Ester carbonyl mole fraction (HYB Basis) (%)	Mean number of poly(lactone) ester units per Mg cation
PLDLA-INSOL	**0.30**	**22.4**	**4.9**	**8**
L:C 1:2-INSOL	**0.27**	**15.4**	**3.6**	**7**
L:C 1:1-INSOL	**0.27**	**15.4**	**3.6**	**7**
L:C 2:1-INSOL	**0.29**	**38.0**	**8.8**	**15**
L:V 1:2-INSOL	**0.24**	**28.7**	**6.0**	**13**
L:V 1:1-INSOL	**0.25**	**43.1**	**9.7**	**19**
L:V 2:1-INSOL	**0.27**	**31.0**	**7.1**	**13**

587

588

Table 3. EDAX Results for various insoluble phases and LDH-carbonate (% by mass).

Specimen	Mg	Al	Mg/Al mass ratio
LDH-Carbonate	17.20	7.83	1.98
PLDLA-INSOL	18.21	0.9	20.2
L:C 1:2-INSOL	18.82	10.3	1.83
L:C 1:1-INSOL	16.05	7.12	2.25
L:C 2:1-INSOL	12.65	6.31	2.00
L:V 1:2-INSOL	19.89	10.25	1.94
L:V 1:1-INSOL	17.87	10.40	1.72
L:V 2:1-INSOL	11.89	3.22	3.69

Table of Contents Graphic (for Table of Contents use only)